Loss-induced modal selection by a resistive wiremesh

Svetlana Kuznetsova, Yves Aurégan, Vincent Pagneux

Loss-induced modal selection by a resistive wiremesh

Svetlana Kuznetsova,[a] Yves Aurégan, and Vincent Pagneux[b]
Laboratoire d'Acoustique de l'Université du Mans (LAUM),
UMR 6613, Institut d'Acoustique - Graduate School (IA-GS), CNRS, Le Mans Université,
Avenue O. Messiaen, 72085 LE MANS CEDEX 9, France

This work examines the impact of local losses produced by a resistive wiremesh on the modes of an acoustic cavity. In the 1D case, we demonstrate the ability to selectively affect the modes, ranging from being completely unaffected by the wiremesh to being fully absorbed by it. This effect can be used to filter the cavity modes. In the 2D case, we discuss the effect of wiremesh rotation on the cavity modes. A new type of modes that are localized on the wiremesh with a purely imaginary eigenfrequency has been identified. These findings show that wiremeshes are ultrabroadband lossy metasurfaces offering a simple and straightforward way to explore passive non-Hermitian systems.

[https://doi.org(DOI number)]

[XYZ] Pages: 1–8

I. INTRODUCTION

The study of non-Hermitian systems has gained significant attention in recent years due to their potential applications in wave control (Ghatak *et al.*, 2020; McDonald and Clerk, 2020; San-Jose *et al.*, 2016). Losses can be used not only to absorb waves, as is traditionally done (Huang *et al.*, 2023; Mei *et al.*, 2012; Merkel *et al.*, 2015; Wang *et al.*, 2023; Yang and Sheng, 2017), but also to improve transmission in some cases (Cerjan and Fan, 2016).

Metamaterial absorbers that use subwavelength resonators can provide up to perfect absorption near the resonance frequencies when carefully adjusted parameters are used (Romero-García *et al.*, 2016), making them useful for controlling waves in a duct or in a cavity. One potential drawback of this application of the subwavelength resonators is that its effectiveness is limited to a narrow frequency range centered around the metamaterial resonance frequency.

In the case of a cavity, it may be beneficial to control multiple modes. To achieve this, a subwavelength device that is active over a wide range of frequencies is required. Broadband absorption can be achieved by avoiding resonance, as demonstrated by metallic conductive films (Li *et al.*, 2015; Nimtz and Panten, 2010) which allow for total absorption using the concept of coherent perfect absorption (CPA). Similarly, ultrathin millimetric resistive sheets offer the same potential in the field of airborne acoustics (Coutant *et al.*, 2020; Farooqui *et al.*, 2022; Ingard, 2009). Often referred to as wiremesh, these resistive sheets are efficient across a wide range of frequencies, including static flow applications such as filtration. They maintain their efficiency at high frequencies as long as the wavelength is larger than the thickness of the mesh. Resistive sheets can be viewed as ultra-thin non-Hermitian metasurfaces.

In this paper, we present the impact of the resistive wiremesh inserted inside the acoustic cavity on the wavenumbers and structure of its modes. We first focus on the 1D case and derive the dispersion relation and the following properties of the trajectories of the wavenumbers in the complex plane with the variation of the wiremesh impedance. As the losses are localized, the modal behavior is expected to strongly depend on the position of the wiremesh. This study complements the findings of reference Farooqui *et al.*, 2022, which only analyses the wiremesh at the centre of the cavity. Next, we will consider the 2D case, where additional degrees of freedom are introduced to affect the modes. These degrees of freedom include the rotation of the wiremesh and the aspect ratio of the cavity. Incidentally, we will demonstrate that the wiremesh supports a new type of mode, which we refer to as "extraordinary viscous modes". These modes are located around the resistive metasurface and have a purely imaginary wavenumber.

II. MODES OF THE 1D CAVITY WITH AN INSERTED WIREMESH

A. Dispersion equation

We consider the eigenmodes of a cavity of length L with Neumann boundary conditions on the walls and an embedded wiremesh placed at $x = d$ (Fig. 1). The cavity if filled with air characterized by the speed of sound c_0 and density ρ_0. At $x \in [0, d[$ (region 1) and $x \in]d, L]$ (region 2) the pressure obeys the Helmholtz equation (con-

[a] Now at Univ. Lille, CNRS, Centrale Lille, Junia, Univ. Polytechnique Hauts-de-France, UMR 8520 - IEMN - Institut dElectronique de Microelectronique et de Nanotechnologie, F-59000 Lille, France
[b] vincent.pagneux@univ-lemans.fr

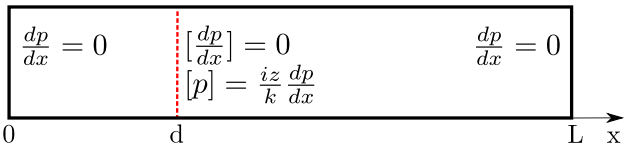

FIG. 1. 1D cavity with a wiremesh (red dashed line).

vention $\exp(-i\omega t)$)

$$\frac{d^2p}{dx^2} + k^2 p = 0 \tag{1}$$

with $dp/dx = 0$ at $x = 0$ and $x = L$, and where $k = \omega/c_0$ is the wavenumber and ω the frequency. The wiremesh is a very thin resistive sheet responsible for the dissipation; it is typically made of stainless-steel fabric of less than one millimeter thickness (Coutant *et al.*, 2020; Farooqui *et al.*, 2022; Ingard, 2009). It supports the continuity of the velocity (and consequently the derivative of the pressure) and introduces a pressure drop as

$$p_2(d^+) - p_1(d^-) = \frac{iz}{k}\frac{dp_{1,2}}{dx}(d), \qquad \left.\frac{dp_2}{dx}\right|_{d^+} = \left.\frac{dp_1}{dx}\right|_{d^-}, \tag{2}$$

where z is the impedance normalized by $\rho_0 c_0$. The resistance z is a positive real number (remarkably independent of the frequency as long as the wavelength is much larger than the mesh thickness) that characterizes the lossy effect of the wiremesh and which "microscopically" originates from the viscous friction of the oscillatory acoustic creeping flow in the pores. With equations (1), (2) and hard wall boundary conditions we have the eigen-problem of the cavity with wiremesh, with eigenvalues k and eigenmodes p. Note then that, if k is an eigenvalue, so is $-k^*$ (where * means complex conjugation), a property reminiscent of the non-Hermitian particle-hole symmetry recently studied for systems with loss and gain (Ge, 2017). This property will be of peculiar interest for the "extraordinary viscous modes" with purely imaginary wavenumbers that will appear in the following; indeed due to this $k \to -k^*$ symmetry they are robust in the sense that they can leave the imaginary axis only when coalescing.

When $z = 0$ we have the modes of an empty cavity with the wavenumbers $k_{0n} = \pi n/L$. In the opposite case when $z = \infty$ the wiremesh corresponds to an hard wall and we have two separated cavities of lengths d and $L-d$ with eigenfrequencies $k_{1n} = \pi n/d$ and $k_{2n} = \pi n/(L-d)$ correspondingly. Without loss of generality, we will consider in the following that $d < L/2$ and thus we refer to the sub-cavity of the length d (region 1) as a small one, and to the sub-cavity of the length $L-d$ (region 2) as the large one.

When the resistance of the wiremesh varies between these two limiting cases ($z \in]0, \infty[$), the solutions of the Helmholtz equation in each sub-cavities take the form

$$p_n(x) = \begin{cases} p_{1n}(x) = A_{1n}\cos(k_n x) & x \in [0, d[\\ p_{2n}(x) = A_{2n}\cos(k_n(x-L)) & x \in]d, L] \end{cases} \tag{3}$$

Then, using the coupling conditions (2) we obtain

$$\begin{aligned} &A_{1n}\sin(k_n d) = A_{2n}\sin(k_n(d-L)), \\ &A_{1n}\cos(k_n d) - A_{2n}\cos(k_n(d-L) = izA_{1n}\sin(k_n d)), \end{aligned} \tag{4}$$

which leads to the following dispersion relation

$$D(k) = \sin(k_n L) + iz\sin(k_n d)\sin(k_n(d-L)) = 0. \tag{5}$$

The unknown of this equation is the complex wavenumber k_n which is a function of z and d. Fixing d and increasing z from 0 to ∞ one should obtain the evolution of k_n from k_{0n} to one of the k_{1p} or k_{2p}.

B. Wiremesh in the middle of the cavity

We first remind here the results when the wiremesh is in the middle of the cavity ($d = L/2$)(Farooqui *et al.*, 2022). In this particular case, due to the symmetry of the problem all the modes can be divided into the symmetric and anti-symmetric ones. The solutions for the symmetrical modes are not perturbed by the wiremesh since they have a zero derivative in the middle of the cavity (zero acoustic velocity is not producing friction at the wiremesh). The mode wavenumbers without loss are preserved and remain on the real axis. On the opposite, the solutions for the antisymmetric modes are strongly affected by the wiremesh as its impedance grows: they acquire an infinite imaginary part for the very specific value $z = 2$. It means that, for this very specific value of the impedance, the antisymmetric modes are completely absorbed by anechoicity. For $z > 2$, the mode wavenumbers reappeared in the form of an antisymmetric combination of eigenmodes of the left and right sub-cavities (Farooqui *et al.*, 2022) which approach the real axis when $z \to \infty$.

C. Wiremesh not in the middle of the cavity

In the case $d < L/2$, the symmetry of the cavity is broken and generically all the mode wavenumbers are leaving the real axis as z is increased from zero, visiting in the lower half complex plane (the lossy region with the chosen convention $\exp(-i\omega t)$). Similarly to the symmetric case, the behavior of complex wavenumbers can be split into two types of trajectories (Fig. 2): i) the continuous one (in black) displaying a typical resonance trapping behavior (Dittes, 2000; Persson *et al.*, 1998, 2000) that forms an open loop, first leaving the real axis but then returning back to it and being less absorbed when increasing the loss, ii) the trajectories (in red and blue) which acquire an infinite $\mathrm{Im}(k)$ as $z = 2$, infinitely absorbed, and then reappear and return to the real axis. Surprisingly, there is a critical impedance value which is the same ($z = 2$) as in the symmetric cavity where some

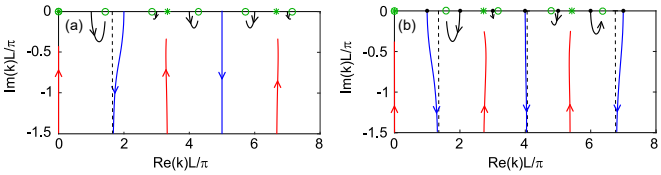

FIG. 2. Curves of k in the complex plane obtained by changing z in the calculation of wavenumbers for (a) $d = 0.3L$ and (b) $d = 0.37L$. The green circles (k_{2n}) and asterisks (k_{1n}) correspond to their final positions at $z \to \infty$. The blue lines are the trajectories which go to $\mathrm{Im}(k) \to -\infty$ as $z \to 2^-$, the red ones are the returning trajectories coming from $\mathrm{Im}(k) \to \infty$ as $z \to 2^+$.

mode wavenumbers go to infinity. It will be discussed in the next subsection.

The numerical solutions of the equation (5) are shown in Fig. 2 for (a) $d = 0.3L$ and (b) $d = 0.37L$, $z \in [0, 5]$ where the green asterisks and circles correspond to k_{1n} and k_{2n}. All wavenumbers begin their trajectories vertically in the k-plane because in the vicinity of $z = 0$, the wavenumber is given by

$$k_n L = \pi n + i\frac{z}{2}(\cos(2\pi n d/L) - 1) + O(z^2). \qquad (6)$$

where $z \ll 1$.

The trajectories that remain finite return on the real axis (resonance trapping) as a solution for the large subcavity k_{2n} when $z \to \infty$. We observe that the k_{0n} solution at $z = 0$, having a finite continuous trajectory, evolves towards the nearest sub-cavity solution on the real axis as z increases. The closeness between the initial k_{0n} and final k_{1n}, k_{2n} is determined by the position d of the wiremesh. Changing d, one changes the distance between the initial and final wavenumbers, which is accompanied by the interchanges of the trajectories behaviors. This is seen from the comparison of Fig. 2(a) and (b). In (a) the trajectory of the first mode of the empty cavity is finite, while in (b) it goes to infinity and its place is taken by the second mode. The dashed black lines are the vertical asymptotes

In Fig. 3 is shown the evolution of the profiles of the mode of Fig. 2(b) ($d = 0.37L$) when z is going from 0 (no wiremesh) to $+\infty$ (rigid wall limit). Each column corresponds to the 5 lowest order modes for different values of z labeled at the top of each column. For $z = 0$, one obviously observes the modes of the empty cavity. The arrows between the plots help to follow by continuity each mode individually as z is growing. To remove the ambiguity introduced by the solutions passing through infinity and to be able to track the modes validly, we have regularized the problem by introducing a very small tilt of the wiremesh in a 2D problem. Indeed, as we shall see in Section III), no solution then goes to infinity but only takes a larsge value of $\mathrm{Im}(k)$.

Very close to the singular behavior, for $z = 2 \pm 0.0025$, some modes (Fig. 3(g,l,n)) appear to be located at the wiremesh (whose position of is indicated by a dotted black vertical line). We are facing the singular modes disappearing at $z = 2$. For $z \to \infty$ (Fig. 3(p-t)), $k_n \to k_{1p}$ or k_{2p} and the mode is localized in one of the two subcavities if $k_{1p} \neq k_{2p}$.

1. Modes with infinite $\mathrm{Im}(k)$

When $z \to 2$, for the singular modes, the diverging imaginary part of k can be approximated by $\mathrm{Im}(k) \approx \frac{1}{2d}\ln|z/2 - 1|$ and consequently their characteristic localization length can be introduced as $l_l = 1/\mathrm{Im}(k) = 2d/\ln|z/2 - 1|$. The mode is becoming more and more confined with $z \to 2$ and completely disappears at $z = 2$ with $l_l = 0$.

In order to get some hints about this singular behavior, let us propose an heuristic analysis of the mode structure. First we can remark that each mode p_n can be separated into an odd (subscript o) and an even (subscript e) part with respect to $x = d$:

$$p_{on} = \begin{cases} \frac{1}{2}\sin(k_n d)\left(iz\cos(k_n(x-d)) - 2\sin(k_n(x-d))\right), \\ \qquad\qquad \text{when } x < d \\ -\frac{1}{2}\sin(k_n d)\left(iz\cos(k_n(x-d)) + 2\sin(k_n(x-d))\right), \\ \qquad\qquad \text{when } x > d \end{cases} \qquad (7)$$

$$p_{en} = \frac{1}{2}(2\cos(k_n d) - iz\sin(k_n d))\cos(k_n(x-d)). \qquad (8)$$

where it has been chosen that the coefficients $A_{1n} = 1$ in eq. 2. Of course, this decomposition is only defined for $x \in [0, 2d]$.

It can be shown perturbatively that $p_{en} \to 0$ when $z \to 2$ (except the points $x = 0$ where $p_{en} \to 1/4$). On the opposite, the odd parts p_{on} grow exponentially in space toward the wiremesh when $z \to 2$ with $|p_{on}(d^-)| \to (2\sqrt{|z/2-1|})^{-1}$ (while at $x = 0$, $p_{on} = 3/4$). Thus, in the limit $z \to 2$, p_{on} becomes much larger than p_{en} and singular modes are dominantly odd with respect to $x = d$. One can introduce a virtual cavity of length $2d$ and the singular modes are close to the odd eigenmodes of the virtual cavity with $\mathrm{Im}(k) \to -\infty$ and $\mathrm{Re}(k) \to (2n-1)\pi/2d$ (Farooqui *et al.*, 2022). After disappearing at $z \to 2^-$ singular modes reappear for $z \to 2^+$ with $\mathrm{Re}(k) \approx 2n\pi/2d$ and evolve to the eigenmodes of the smaller sub-cavity k_{1n} when $z \to \infty$.

We can remark that the mode exhibited in Fig. 3 (q) corresponds to the one, which came from $\mathrm{Re}(k) = 0$, $\mathrm{Im}(k) = -\infty$ when $z = 2$. Taking into account the relations (3), (4) and putting $z \to \infty$, one obtains that the ratio of the pressures in the large and small subcavities is $d/(L-d)$. For $z > 2$, it has a purely imaginary wave number and it belong to the family of extraordinary viscous modes that we will described in Section III.

Globally, we would like to summarize what we observed for the evolution of the spectrum when going from no wiremesh ($z = 0$) to opaque wiremesh ($z \to +\infty$). When the wavenumber k eigenvalue remains finite for

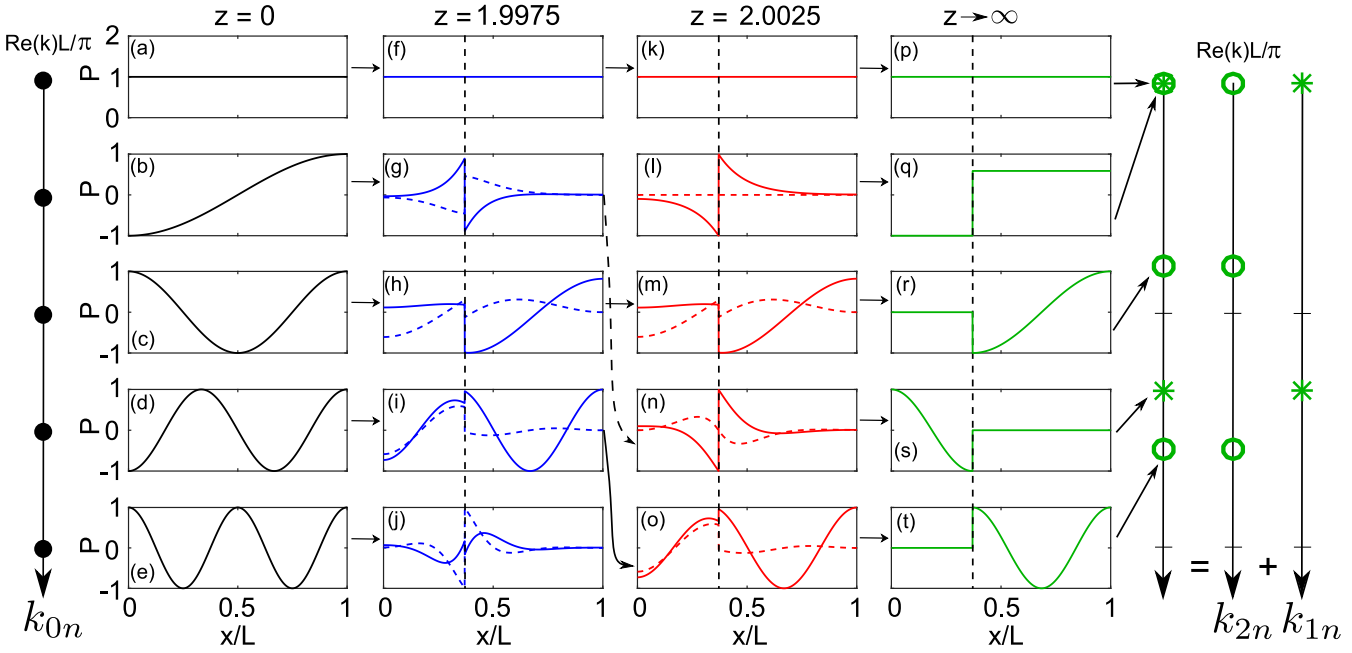

FIG. 3. The pressure profiles (solid lines – real part, dashed lines – imaginary part) of the lowest order eigenmodes of the cavity for different values of z. Left and right bars – the initial ($z = 0$) and final ($z \to \infty$) spectra. The dashed line indicates the position of the wiremesh. The arrows indicate the evolution of the modes with the increase of z.

any z (displaying a resonance trapping behavior), it is tending for $z \to +\infty$ to a mode in the large cavity (k_{2n}). For the eigenvalues that are diverging for $z \to 2$, in contrast, they are tending to a mode of the small cavity (k_{1n}) when $z \to +\infty$. We have observed this behaviour for all the cases we have studied and it remains for us an open problem to explain it.

2. Exceptional points of the spectrum

The form of the dispersion relation (5) allows us to expect some peculiarities if the ratio d/L is rational. Indeed, it can be shown that, if $d/L = m/n$ with $m, n \in \mathbb{N}$, then the spectrum of the eigenvalues k is periodic in the direction parallel to the Re(k)-axis with the period $n\pi/L$ and is additionally mirror symmetric with respect to $pn\pi/2L$ where $p \in \mathbb{Z}$ (for more details, see Appendix B and C in the supplementary material). It is illustrated in Fig. 4 for $d/L = 1/3, 1/4, 2/5$ with the periods of the patterns thus equal to Re(k)L/π = 3, 4 and 5 respectively.

It appears that this structure and symmetry of the spectrum make it possible to obtain exceptional points (EPs) with $d/L = m/n$ and additional restriction on m and n. To find these EPs, we use the property that they are double solution of the dispersion relation (5) and hence correspond to the solutions k_{EP} of the system

$$\begin{aligned} D(k) &= 0, \\ D'(k) &= 0. \end{aligned} \tag{9}$$

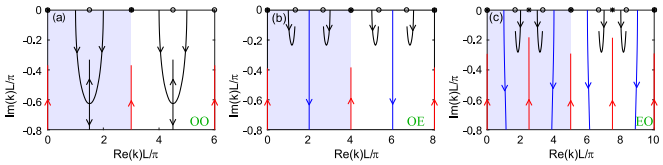

FIG. 4. Trajectories of the complex wavenumbers for (a) $d = L/3$, (b) $d = $ L/4, (c) $d = $ 2L/5, the shaded area corresponds to one period of the trajectory pattern. The green letters correspond to the m/n ratio – Odd-Odd, Odd-Even, Even-Odd.

It can be shown that the real parts of k_{EP} satisfy the following equations (see Appendix A in the supplementary material)

$$\begin{aligned} \mathrm{Re}(k_{EP})(L - 2d) &= \pi/2(2p + 1), \\ \mathrm{Re}(k_{EP})2d &= \pi(2m + 1), \end{aligned} \tag{10}$$

with $p, m \in \mathbb{N}$. Eliminating Re(k_{EP}) for these last equations, it leads to the following condition for the position d of the wiremesh in order EPs to exist:

$$d_{EP}/L = \frac{2m + 1}{2p + 1 + 2(2m + 1)} = \frac{M}{N}, \tag{11}$$

being the particular ratio of *two odd numbers* $M = 2m+1$ and $N = 2p + 1 + 2(2m + 1)$. At an EP, using eq. (11), we have also that

$$\mathrm{Re}(k_{EP})L/\pi = (2m + 1) + p + 1/2. \tag{12}$$

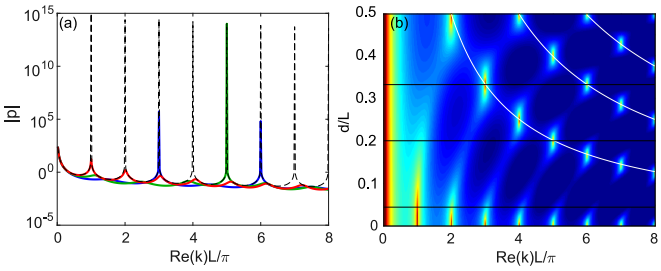

FIG. 5. (a) Pressure in the cavity excited by the point source at $x = 0$ for $z = 0$ (black dotted line), $z = 2$ and $d = L/3$ (blue), $d = L/5$ (green) and $d = L/25$ (red), (b) $\log(|p|)$ measured at $x = L$. The black lines correspond to d/L from (a).

From the illustrative point of view, the situation is depicted on Fig. 4 (a) for $d/L = 1/3$ when varying the resistance z from 0 to $+\infty$. The spectrum has the period $3\pi/L$ and the EPs are appearing for $\mathrm{Re}(k_{EP}) = (3/2 + p)\pi/L$ with $p = 0, 1, 2, \ldots$.

In contrast to what described previously, when the d/L is not a ratio of odd/odd numbers, the EPs do not occur, as is illustrated on Fig. 4 (b), (c) for $d/L = 1/4$ (ratio odd/even) and $d/L = 2/5$ (ratio even/odd). Remark that since the 0-th mode does not "feel" the wiremesh, the same insensitivity applies to the $(n+1)$-st modes due to the periodicity.

At this point, it is important to note that the characteristics of the studied wavenumber eigenvalues can effectively select cavity modes. Indeed, by simply changing the position d one can select the desired modes (with zero imaginary wavenumber) to be unperturbed by the wiremesh while all the others will be absorbed. To investigate this phenomenon, we take a point source positioned at $x = x_0$ in the cavity and we solve the Helmholtz equation

$$d^2p/dx^2 + k^2p = Q\delta(x - x_0).$$

It is the Green function response. The resulting pressure can then be expressed as follows:

$$p(x) = \begin{cases} p_1(x) = A_1\cos(kx), & x \in [0, x_0[, \\ p_2(x) = A_2\cos(k(x-d)) + B_2\sin(k(x-d)), & x \in [x_0, d[, \\ p_3(x) = A_3\cos(k(x-L)), & x \in]d, L]. \end{cases}$$

The additional boundary conditions at $x = x_0$ read

$$p_2(x_0) = p_1(x_0), \quad p_2'(x_0) - p_1'(x_0) = Q. \tag{13}$$

If one measures the pressure at the right end $x = L$, putting the point source at the left end $x_0 = 0$ one obtains

$$p_3(L) = \frac{Q}{kD(k)} \tag{14}$$

with $D(k)$ given by the dispersion relation eq. 5. This is illustrated in Fig. 5(a) where we plot $p_3(L)$ as a function of the wavenumber for $z = 2$. The dashed line corresponds to the empty cavity, while the blue and the green lines correspond to $d/L = 1/3$ and $d/L = 1/5$ respectively. Then all the modes, except the 3^{rd} (for $d/L = 1/3$) and the 5^{th} (for $d/L = 1/5$) ones (and their multiples) are strongly suppressed. One might expect that taking a sufficiently large n will lead to the suppression of all the modes in the range $\mathrm{Re}(k)L/\pi \in (1, n-1)$, which would conflict with the fact that as $d \to 0$ we should restore the empty cavity modes. Actually, the decrease in selection efficiency with the decrease of the ratio d/L is resolving this apparent paradox, and Figure 5(a) shows the case where d/L = 1/25, represented by the red curve, where the peaks of the suppressed modes are not so well suppressed and still noticeable.

In Fig. 5(b), that gives a global point of view, we plot the pressure ($\log(|p|)$) defined in eq. (14) as a function of d/L and $\mathrm{Re}(k)$, where the lines in figure (a) correspond to the horizontal cuts to the plot (black lines). We see the bright sharp peaks attributed to the modes insensitive to the wiremesh. As d decreases, the residues of the empty cavity modes become more evident, as shown in Fig. 5(a). The white hyperbolas represent the dependence $d/L = n/(kL/\pi)$ corresponding to the cancellation of the derivative of the pressure at the wiremesh in the empty cavity, i.e. the case where the acoustic mode is not feeling the mesh if in addition it is satisfying $k(L - d) = m\pi$ with m integer.

III. MODES OF A 2D CAVITY WITH AN INSERTED WIREMESH

Now, to expand our investigation, leaving the 1D case, we are going to examine a 2D cavity with hard walls (Neumann boundary conditions) and a wiremesh in the centre (see Fig. 6 (a)).

When the wiremesh is aligned with the y-axis, the problem is a separable variable problem and we have symmetric and anti-symmetric modes with respect to $x = L/2$ just like in the analogous 1D case (Farooqui *et al.*, 2022). The symmetric modes do not feel the wiremesh and they remain the same as in the empty cavity. We will thus focus on the anti-symmetric wavenumber eigenvalues that leave the real axis in the complex plane. The dispersion relation for these anti-symmetric modes is:

$$\cot(k_xL/2) = \frac{iz}{2k}k_x, \tag{15}$$

where $k^2 = k_x^2 + (n\pi/h)^2$.

The pressure distribution for the initial resistance $z = 0$ shown in the eigenvalue trajectories is $p(x, y) = A\cos(n\pi/L)\cos(m\pi/h)$ with $n, m \in \mathbb{N}$. The modes that are uniform along the y-axis ($m = 0$) correspond to those studied in the previous section for the 1D case, and we will omit them in the following. The trajectories of the modes with $m = 1$ are shown in Fig. 6(b). The symmetric modes with respect to the horizontal x axis (even n) do not feel the wiremesh and stay on the real axis (circles in Fig. 6(b)). The modes with odd n are anti-symmetric

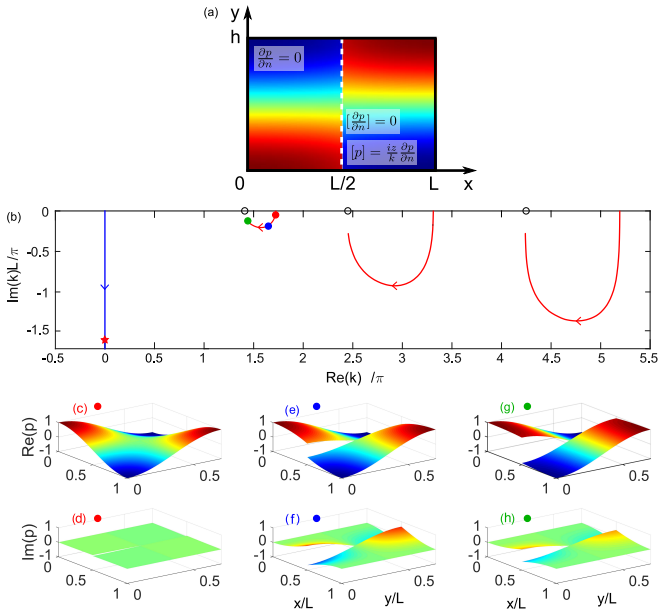

FIG. 6. (a) Geometry of the 2D cavity with an inserted wiremesh, (b) trajectories of the complex wavenumbers of the modes $(m, 1)$ for $h/L = \sqrt{5}/\pi$. The Re(p) and Im(p) fields of the initial $(1, 1)$ mode for (c), (d) $z = 0.1$, (e), (f) $z = 2.5$, (g), (h) $z = 5$.

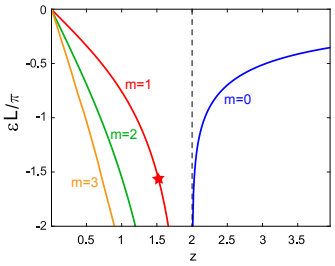

FIG. 7. Solutions of the eq. 17 as functions of z. The modes numbers $m = 0$, 1, 2, 3 are labeled next to the corresponding curves. The red star indicates the extraordinary viscous mode for $m = 1$ and $z = 1.5$.

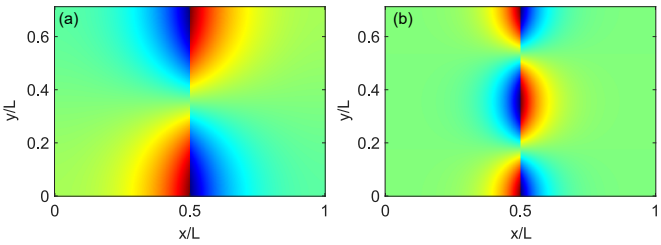

FIG. 8. Spacial distributions of p for (a) $m = 1$, (b) $m = 2$ modes with a purely imaginary k for $z = 1.5$.

and move away from the real axis as z increases, becoming anti-symmetric counterparts of the corresponding symmetric modes with the same wavenumber. The higher is n the greater imaginary part the trajectory acquires due to the increase of $\partial p/\partial x$. In Fig. 6 (c) - (h) we plot the real and imaginary parts of pressure spacial distribution for the mode (1,1) at the points marked by the colored dots on the trajectory. We observe the evolution of the x-axis dependence forming a clear discontinuity at the wiremesh, while the y-axis dependence remains the same.

It is important to note that, in a novel and unexpected way, there are an infinite number of "extraordinary viscous modes" whose wavenumber eigenvalues are purely imaginary. To look for those modes, we can write

$$k^2 = k_x^2 + (\pi m/h)^2 = -\varepsilon^2, \tag{16}$$

from which we can see that $k_x = i\gamma$ is purely imaginary as well. Then the pressure takes the form $p(x, y) = A\cos(m\pi y/h)\cosh(\gamma x)$. Then the dispersion relation (15) for these anti-symmetric modes reads:

$$\cot(\gamma L/2) = -\frac{\gamma z}{2\varepsilon}. \tag{17}$$

For each $m \geq 1$, this equation has a single solution in the range of z in $[0, 2]$. They lead to imaginary wavenumbers going to $-\infty$ on the imaginary axis as z increases from 0 to 2^-. In contrast, for $m = 0$ there is only a solution for $z > 2$. The corresponding wavenumber comes up the imaginary axis to become a flat mode when $z \to \infty$. This is illustrated in Fig. 7 for several lowest order modes, where the red star is the case $m = 1$ for $z = 3/2$ displayed as well in Fig. 6(b).

The spatial pressure distribution of the modes $m = 1$ and $m = 2$ is shown in Fig. 8, the case (a) matches the star in Fig. 7. They are localized at the wiremesh and the localization length decreases with the increase of m. The trajectory of the mode $m = 1$ is shown as a blue line in Fig. 6 for $z < 2$, the pressure field in Fig. 8(a) corresponds to the red star on the line.

To generalize our study, we now consider a non-separable 2D geometry where the wiremesh is tilted at an angle of α as shown in Fig. 9(a). Then, to find the spectrum of the cavity, separation of variables is not anymore possible and some coupling should be observed between the decoupled modes observed previously (i.e. between modes with m=1,2,,3...). In Fig. 9(b) we plot the trajectories of the wavenumber eigenvalues k when varying z, for $\alpha = 0.1$ rad. The modes that previously, when $\alpha = 0$, had Im(k) tending towards infinity, now remain finite even though Im(k) can still take large negative values, and they return to the real axis as $z \to \infty$. Furthermore, the modes that were previously unaffected by the wiremesh now depart from the real axis: unsurprisingly, now all the modes are influenced by the presence of the losses. The real and imaginary parts of pressure distributions are shown in Fig. 9(c) - (j) at the points on the trajectory (1,0) marked by the colored dots. Starting from the continuous distribution at $z = 0$ the mode rapidly develops a discontinuity in both Re(p) and Im(p) and mimics the behavior of the corresponding anti-symmetric

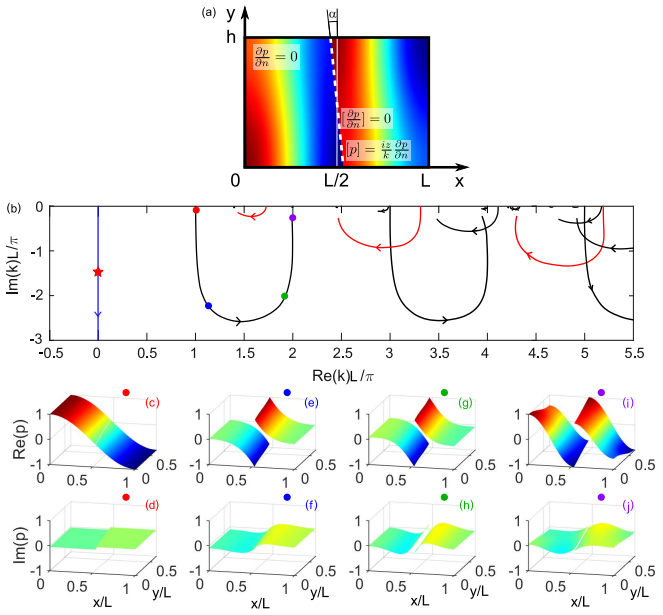

FIG. 9. (a) Geometry of the 2D cavity with an inserted tilted wiremesh, (b) Trajectories of the complex wavenumbers of the cavity for $\alpha = 0.1$ rad, $h/L = \sqrt{5}/\pi$. The Re(p) and Im(p) fields of the initial $(1, 1)$ mode for (c), (d) $z = 0.1$, (e), (f) z = 2, (g), (h) z = 2.01, (i), (j) z = 5.

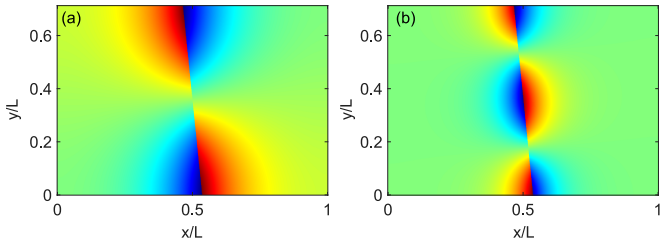

FIG. 10. Spacial distributions of p for (a) m = 1, (b) m = 2 modes with a purely imaginary k for z = 1.5 when the wiremesh is tilted.

mode for $\alpha = 0$. Additional results are given in Appendix D in the supplementary material for a tilted wiremesh that is not in the middle of the cavity, breaking all the spatial symmetry of the problem.

Interestingly, even when the wiremesh is tilted, there are again "extraordinary viscous modes" with purely imaginary k (Re(k) = 0). Indeed, they are protected by the $k \to -k^*$ symmetry of the spectrum as long as the value of the angle α is not large enough to provoke the coalescence of two of them to leave the imaginary axis. Their pressure distributions are shown in Fig. 10 for $m = 1$ and $m = 2$. They replicate the behavior of their analogues at $\alpha = 0$ by being localized near the wiremesh. The results demonstrate that the "extraordinary viscous modes" remain robust and unaffected even with a slight tilt of the wiremesh. Overall, these modes look similar to surface plasmon modes (Maier *et al.*, 2007).

IV. CONCLUSIONS

In this work we have studied the impact of localized losses represented by a flat wiremesh on the eigenmodes of an acoustic cavity in one and two-dimensional configurations. By varying the position and impedance of the wiremesh, the cavity natural frequencies have very rich and diverse behavior the complex plane with negative imaginary part. Some of these modes may have a very large or even infinite negative imaginary part of the wavenumber. Other modes are able to keep low loss due to resonance trapping behavior. This study demonstrates that absorption efficiency is non-monotonic with respect to impedance. At the very specific value of $z = 2$, certain modes are entirely absorbed, regardless of the symmetry of the problem. By adjusting the wiremesh position, it is possible to select the modes that remain undisturbed while absorbing all others. This technique is an effective tool for filtering cavity modes.

In the 2D case, the tilt of the wiremesh may be used as an additional degree of freedom to affect the modes. However, it is important to note that no modes undergo complete absorption in this case. Instead, they leave the real axis and return as the impedance of the wiremesh grows. Despite this, tuning the impedance of the wiremesh remains an efficient tool for selectively manipulating the absorption of modes. This demonstrates the robustness of this filtering technique.

Finally, a new type of cavity mode with a purely imaginary wavenumber has been identified. These "extraordinary viscous modes" are robust due to the $k \to -k^*$ symmetry of the spectrum and they are spatially localized close to the wiremesh and decrease exponentially as they move away from it.

ACKNOWLEDGMENTS

This work was supported by the French National Agency for Research (SelfiXs Project, ANR-18-CE92-0001). The authors have no conflicts of interest to declare. The data that support the findings of this study are available from the corresponding author upon reasonable request.

Cerjan, A., and Fan, S. (**2016**). "Eigenvalue dynamics in the presence of nonuniform gain and loss," Physical Review A **94**(3), 033857.

Coutant, A., Aurégan, Y., and Pagneux, V. (**2020**). "Anomalous transmission through periodic resistive sheets," The Journal of the Acoustical Society of America **147**(5), 3124–3135.

Dittes, F.-M. (**2000**). "The decay of quantum systems with a small number of open channels," Physics Reports **339**(4), 215–316.

Farooqui, M., Aurégan, Y., and Pagneux, V. (**2022**). "Ultrathin resistive sheets for broadband coherent absorption and symmetrization of acoustic waves," Physical Review Applied **18**(1), 014007.

Ge, L. (**2017**). "Symmetry-protected zero-mode laser with a tunable spatial profile," Physical Review A **95**(2), 023812.

Ghatak, A., Brandenbourger, M., Van Wezel, J., and Coulais, C. (**2020**). "Observation of non-hermitian topology and its bulk–

edge correspondence in an active mechanical metamaterial," Proceedings of the National Academy of Sciences **117**(47), 29561–29568.
Huang, S., Li, Y., Zhu, J., and Tsai, D. P. (**2023**). "Sound-absorbing materials," Physical Review Applied **20**(1), 010501.
Ingard, U. (**2009**). *Noise reduction analysis* (Jones & Bartlett Publishers).
Li, S., Luo, J., Anwar, S., Li, S., Lu, W., Hang, Z. H., Lai, Y., Hou, B., Shen, M., and Wang, C. (**2015**). "Broadband perfect absorption of ultrathin conductive films with coherent illumination: Superabsorption of microwave radiation," Physical Review B **91**(22), 220301.
Maier, S. A. *et al.* (**2007**). *Plasmonics: fundamentals and applications*, **1** (Springer).
McDonald, A., and Clerk, A. A. (**2020**). "Exponentially-enhanced quantum sensing with non-hermitian lattice dynamics," Nature communications **11**(1), 5382.
Mei, J., Ma, G., Yang, M., Yang, Z., Wen, W., and Sheng, P. (**2012**). "Dark acoustic metamaterials as super absorbers for low-frequency sound," Nature communications **3**(1), 756.
Merkel, A., Theocharis, G., Richoux, O., Romero-García, V., and Pagneux, V. (**2015**). "Control of acoustic absorption in one-dimensional scattering by resonant scatterers," Applied Physics Letters **107**(24).
Nimtz, G., and Panten, U. (**2010**). "Broad band electromagnetic wave absorbers designed with nano-metal films," Annalen der Physik **19**(1-2), 53–59.
Persson, E., Gorin, T., and Rotter, I. (**1998**). "Resonance trapping and saturation of decay widths," Physical Review E **58**(2), 1334.
Persson, E., Rotter, I., Stöckmann, H.-J., and Barth, M. (**2000**). "Observation of resonance trapping in an open microwave cavity," Physical review letters **85**(12), 2478.
Romero-García, V., Theocharis, G., Richoux, O., and Pagneux, V. (**2016**). "Use of complex frequency plane to design broadband and sub-wavelength absorbers," The Journal of the Acoustical Society of America **139**(6), 3395–3403.
San-Jose, P., Cayao, J., Prada, E., and Aguado, R. (**2016**). "Majorana bound states from exceptional points in non-topological superconductors," Scientific reports **6**(1), 21427.
Schmidt, K., Semin, A., Thöns-Zueva, A., and Bake, F. (**2018**). "On impedance conditions for circular multiperforated acoustic liners," Journal of Mathematics in Industry **8**, 1–20.
Wang, T., Gong, C., Zhang, S., Zhu, Y., Long, H., Cheng, Y., and Liu, X. (**2023**). "An acoustic metaliner for ultra-broadband sound absorption," Applied Physics Letters **123**(16).
Yang, M., and Sheng, P. (**2017**). "Sound absorption structures: From porous media to acoustic metamaterials," Annual Review of Materials Research **47**, 83–114.